Title

An Online Brain-Computer Interface Based on SSVEPs Measured From Non-Hair-Bearing Areas.

Journal

IEEE transactions on neural systems and rehabilitation engineering : a publication of the IEEE Engineering in Medicine and Biology Society, 25(1)

ISSN

1534-4320

Authors

Wang, Yu-Te
Nakanishi, Masaki
Wang, Yijun
et al.

Publication Date

2017

DOI

10.1109/tnsre.2016.2573819

Peer reviewed

An Online Brain-Computer Interface Based on SSVEPs Measured From Non-Hair-Bearing Areas

Yu-Te Wang, *Member, IEEE*, Masaki Nakanishi, *Member, IEEE*, Yijun Wang, *Member, IEEE*, Chun-Shu Wei, *Student Member, IEEE*, Chung-Kuan Cheng, *Fellow, IEEE*, and Tzyy-Ping Jung, *Fellow, IEEE*

***Abstract*— Steady state visual evoked potential (SSVEP)-based brain-computer interface (BCI) has gained a lot of attention due to its robustness and high information transfer rate (ITR). However, transitioning well-controlled laboratory-oriented BCI demonstrations to real-world applications poses severe challenges for this exciting field. For instance, conducting BCI experiments usually requires skilled technicians to abrade the area of skin underneath each electrode and apply an electrolytic gel or paste to acquire high-quality SSVEPs from hair-covered areas. Our previous proof-of-concept study has proposed an alternative approach that employed electroencephalographic signals collected from easily accessible non-hair-bearing areas including neck, behind the ears, and face to realize an SSVEP-based BCI. The study results showed that, with proper electrode placements and advanced signal-processing algorithms, the SSVEPs measured from non-hair-bearing areas in off-line SSVEP experiments could achieve comparable SNR to that obtained from the hair-bearing occipital areas. This study extended the previous work to systematically investigate the costs and benefits of non-hair SSVEPs. Furthermore, this study developed and evaluated an online BCI system based solely on non-hair EEG signals. A 12-target identification task was employed to quantitatively assess the performance of the online SSVEP-based BCI system. All subjects successfully completed the tasks using non-hair SSVEPs with 84.08 $\pm$ 15.60% averaged accuracy and 30.21 $\pm$ 10.61 bits/min averaged ITR. The empirical results of this study demonstrated the practicality of implementing an SSVEP-based BCI based on signals from non-hair-bearing areas, significantly improving the feasibility and practicality of real-world BCIs.**

***Index Terms*— Brain-computer interfaces (BCI), electroencephalogram (EEG), non-hair-bearing electrodes, steady-state visual evoked potential (SSVEP).**

Manuscript received October 20, 2015; revised May 23, 2016; accepted May 25, 2016. Date of publication May 30, 2016; date of current version January 19, 2017. This work was supported in part by the Army Research Laboratory under Cooperative Agreement Number W911NF-10-2-0022, by the UCSD Frontiers of Innovation Scholars Program, by the UCSD IEM Graduate Research Fellowship, by the National Science Foundation under Grant EFRI-M3C 1137279, and by the National Institutes of Health under Grant 1R21EY025056-01. *(Y.-T. Wang and M. Nakanishi contributed equally to this work.). Corresponding author: Tzyy-Ping Jung* (e-mail: jung@sccn.ucsd.edu).

Y.-T. Wang is with the Department of Computer Science and Engineering, Jacobs School of Engineering, University of California San Diego (UCSD), La Jolla, CA 92093 USA, and also with the Swartz Center for Computational Neuroscience, Institute for Neural Computation, and Center for Advanced Neurological Engineering, Institute of Engineering in Medicine, UCSD, La Jolla, CA 92093 USA (e-mail: yute@sccn.ucsd.edu).

M. Nakanishi and T.-P. Jung are with the Swartz Center for Computational Neuroscience, Institute for Neural Computation, and Center for Advanced Neurological Engineering, Institute of Engineering in Medicine, University of California San Diego (UCSD), La Jolla, CA 92093 USA.

Y. Wang is with State Key Laboratory on Integrated Optoelectronics, Institute of Semiconductors, Chinese Academy of Sciences, Beijing 100083, China.

C.-S. Wei is with the Department of Bioengineering, Jacobs School of Engineering, University of California San Diego (UCSD), La Jolla, CA 92093 USA and also with the Swartz Center for Computational Neuroscience, Institute for Neural Computation, and Center for Advanced Neurological Engineering, Institute of Engineering in Medicine, UCSD, La Jolla, CA 92093 USA.

C.-K. Cheng is with the Department of Computer Science and Engineering, Jacobs School of Engineering, University of California San Diego (UCSD), La Jolla, CA 92093 USA.

Digital Object Identifier 10.1109/TNSRE.2016.2573819

I. Introduction

STEADY-STATE visual evoked potential (SSVEP), the brain's natural electrophysiological response to repetitive visual flickering, has been widely used in the fields of neural engineering and neuroscience [1]. In electroencephalogram (EEG)-based brain-computer interfaces (BCIs), the SSVEP-based BCI has attracted much attention due to its advantages of high performance and rapid user training [2], [3].

The performance of SSVEP-based BCIs depends on the level of sophistication in stimulus presentation, multiple target coding, and target identification methods [4]. Recent progress of the stimulus presentation methods allows presenting stable visual flickers at flexible frequencies on a computer monitor or mobile platforms based on refresh rate [5]–[8]. In addition, the efficacy of hybrid frequency and phase coding methods has been demonstrated for increasing the embedded information in each of visual targets [4], [9]. Advanced signal processing techniques have also been proposed to improve the performance of SSVEP-based BCIs. Recently, a canonical correlation analysis (CCA)-based approach has been used widely to detect SSVEPs tagged with frequency coding [10], [11]. To further enhance the performance of target identification, extended CCA-based approaches that incorporate prerecorded individual calibration data [4], [12] and a filter bank method [13] have been proposed in more recent studies. By considering these issues jointly, the performance of SSVEP-based BCIs has been drastically improved in the past few years [14].

Despite the success in improving the accuracy and speed of SSVEP-based BCIs, moving BCI systems from a well-controlled laboratory setting to a real-life environment remains extremely challenging due to the complications of measuring EEG outside well-controlled laboratory settings [15], [16]. Current BCI operations require extensive subject preparation including scalp abrasion, gel application, and tethered electrodes [17]. Developing a truly practical SSVEP-based BCI system evidently requires significant improvements in measuring EEG signals. Some efforts have been made to overcome these technical barriers of the EEG measurement in the past few years [17]–[20]. For instance, studies have shown that dry-contact and noncontact electrodes can avoid the usage of conduct gels [17], [20]. These electrodes can simply be placed over the hair-covered areas to acquire EEG signals from the scalp without requiring skin preparation or conductive gels. However, a major concern over the use of dry, nonprep electrodes for the EEG measurement is that the signal-to-noise rate (SNR) of the acquired signals might not be as good as that obtained from the gel-based wet electrodes. Furthermore, for some clinical applications such as patients lying face up, measuring EEG from the occipital sites would be undoubtedly more difficult either by wet or dry electrodes [21]. Therefore, an alternative approach to robustly measure high-quality SSVEPs becomes imperative. Our recent proof-of-concept study demonstrated that non-hair-bearing areas including neck, face, and behind the ears can be alternative locations to acquire EEGs without requiring skin preparation or the use of conduct gels [22]. The empirical results of the study showed that SSVEPs could be assessed from those non-hair-bearing areas, and more importantly with a proper electrode selection the SNR of the SSVEPs could be comparable or even higher than that obtained by the wet electrodes placed over the occipital areas. However, the study only tested the SNRs of non-hair SSVEPs on a small group of five subjects. The robustness of non-hair SSVEPs was not fully evaluated. Furthermore, the study did not implement an online SSVEP-based BCI system based solely on the non-hair EEG to validate the feasibility of the non-hair BCI.

More recently, we also demonstrated an online SSVEP-based BCI system using in-the-ear EEGs and the system performance reached 16.6 ± 6.55 bits/min [23]. Independently, Norton *et al.* [24] also proposed a soft and curved electrode system that is capable of acquiring EEGs from auricle. The system provided long-term recording of EEG data by intimately attaching the soft electrode to the complex surface of the ear. The result of SSVEP experiment in the study showed an ITR of 12 bits/min. In summary, although the advanced sensing technologies enabled a new apparatus for acquiring EEGs, the resultant ITRs were not nearly as good as those reported in recent high-speed BCI studies based on occipital EEGs [4], [13], [14]. However, because there are considerable differences across the studies using non-hair and occipital EEGs in terms of stimulus coding mechanism, experimental design and setup, electrode positions and subject pools, it is difficult to directly compare results between non-hair and occipital SSVEPs. In other words, the cost and benefits of using non-hair SSVEPs compared to that using the occipital SSVEPs remains unclear. A concurrent recording of both non-hair and occipital SSVEPs for each individual is required to quantitatively compare the differences in BCI performance between two montages.

This study aims to explore the feasibility and benefit of using EEG data from non-hair-bearing areas, along with the aforementioned advanced stimulus-coding and target-identification methods, to develop and test an online SSVEP-based BCI system. We first explored the scalp distributions of the SNRs of the SSVEPs collected from the offline BCI experiments, and then compared the SNRs of SSVEPs measured by different combinations of electrodes placed over four scalp regions, including neck, face, behind-the-ear, and occipital areas. The CCA-based spatial filtering method was then used to enhance the SNRs of SSVEPs. In addition to the offline analysis, an online BCI experiment was conducted to evaluate the performance of a 12-target SSVEP-based BCI using solely non-hair-bearing electrodes. In the online BCI experiments, the aforementioned hybrid frequency and phase coding method and the extended CCA-based methods that incorporate individual training data and filter bank method were used to optimize the BCI performance.

II. Method

A. Experimental Design

A square-shaped visual stimulus (5×5 cm) was coded and flickering (white and black, 100% contrast, the frequencies varied from 9 to 13 Hz with an interval of 1 Hz) at the center of a ViewSonic P810 21-in CRT monitor (ViewSonic Corporation) with a refresh rate of 60 Hz. These frequencies were generated using the frequency approximation approach [5]. Event triggers that indicated the onsets of visual stimuli were sent and synchronized with EEG data in the amplifier. The stimulation program was developed in Microsoft Visual C++ using the Microsoft DirectX 9.0 framework.

Eleven healthy male subjects (24.23 ± 5.1 years old) with normal and corrected-to-normal vision participated in the offline BCI study. They read and signed an informed consent form approved by the Human Research Protections of the University of California San Diego before the experiment. Subjects were seated in a dim room and faced a computer monitor. They were asked to put their head on a chin rest stationed 35 cm from the monitor, as shown in Fig. 1(a).

The experiment consisted of four runs, each run had five trials, each involved a flickering visual stimulus rendering at a different frequency in a random order. For instance, the first run might consist of 11, 10, 12, 9, and 13 Hz, while another run might consist of 12, 10, 11, 9, and 13 Hz, sequentially. Subjects gazed at a 30-s-long flickering target and rested ($\sim$15 s) between trials to prevent visual fatigue. After each run, there was a break for several minutes.

B. Data Acquisition

This study used a 256-channel EEG system (Biosemi, Inc.) to measure high-density EEGs from each of the participants. The electrodes roughly evenly distributed over the entire head, including face, behind-the-ear, and neck areas, as shown

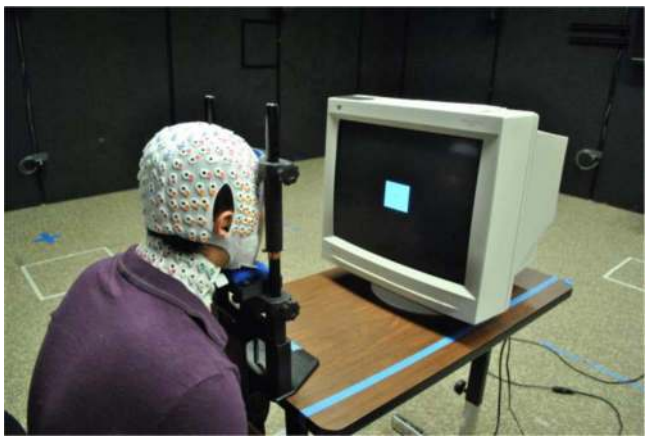

Fig. 1. Subject wore a 256-channel EEG recording system (includes a cap and a neck band) and gazed at a visual stimulus with his head resting on a chin rest. Note that all the cables were removed temporarily in order to have a clean view.

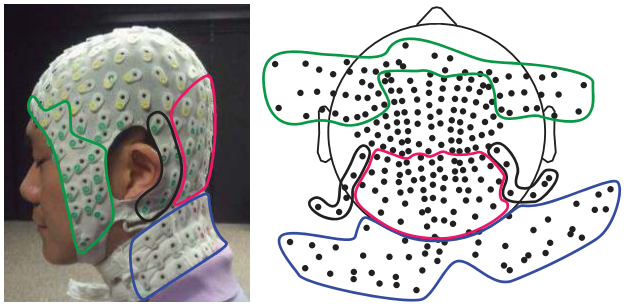

(a) (b)

Fig. 2. (a) Subject wore a 256-channel EEG cap including a neck band. The red, black, green, and blue circles roughly delineate the occipital, behind-the-ear, face, and neck areas, respectively. Note that one or two external electrodes were inserted into the gap between behind-the-ear and EEG cap since the cap might not fit each individual's head. (b) The electrode distribution in a 2-D top view. Again, the red, black, green, and blue circles delineate the occipital, behind-the-ear, face, and neck areas, respectively. Note that this is an approximate 2-D plotting for all electrodes so the actual electrode locations might deviate slightly. The figures were adapted with permission from [22, Fig. 1].

in Fig. 2(a). Note that since the cap cannot perfectly fit an individual subject's head, several extra electrodes were inserted into the gap between the cap and behind-the-ear areas. Fig. 2(b) also shows the 2-D top view of the montage covering the face (green), behind-the-ear (black), occipital (red), and neck (blue) areas. All measured signals were amplified and digitized at a sample rate of 2048 Hz, and referenced to the middle of the forehead. The electrode locations were recorded with a 3-D digitizer (Polhemus, Inc.).

C. EEG Data Analyzing

1) Signal Characteristic Evaluation: The 256-channel EEG data were first down-sampled to 256 Hz and then band-pass filtered from 5 to 50 Hz to investigate the characteristics of the fundamental and harmonic SSVEP components. Each 30-s-long trial was cut into six to seven 4-s-long epochs according to the event codes generated by the stimulus program. The epochs that were contaminated by severe movements, such as eye blink, were manually removed. The remaining trials formed a dataset.

For each recorded channel, the fast Fourier transform (FFT) was applied to the 4-s-long EEG data of all 256 channels to calculate the amplitude spectrum $F(f)$ at frequency f. The SNR of SSVEP at a single channel is defined as the ratio of $F(f)$ to the mean amplitude of the K neighboring frequencies [25]

$$\mathrm{SNR} = \frac{K \times F(f)}{\sum_{k=1}^{K/2} [F(f + k\Delta f) + F(f - k\Delta f)]} \tag{1}$$

where f is the frequency of interest, Δf is the frequency resolution (0.25 Hz in this study), and K is set to 12. This study focused on the scalp distribution (topography) of the SNRs of SSVEPs. The scalp topography maps of multichannel SSVEPs were plotted using the topoplot function in the EEGLAB toolbox [26].

Recent studies reported that spatial filters based on CCA could improve the SNR of SSVEPs [10], [11]. This study thus applied CCA-based spatial filters to maximize the SNR for each defined area. In general, CCA produces two weight matrices that maximize the correlation between the two projected vectors. For instance, consider the two datasets $\boldsymbol{x}$ and $\boldsymbol{y}$ that can be represented by $\boldsymbol{X} = \boldsymbol{w}_x^T \boldsymbol{x}$, and $\boldsymbol{Y} = \boldsymbol{w}_y^T \boldsymbol{y}$, where $\boldsymbol{w}_x^T$ and $\boldsymbol{w}_y^T$ are linear coefficients, and $\boldsymbol{X}$, $\boldsymbol{Y}$ are canonical variables, respectively. We attempt to find the maximum correlation ρ between $\boldsymbol{X}$ and $\boldsymbol{Y}$ by solving

$$\begin{aligned} \rho &= \frac{E[\boldsymbol{X}\boldsymbol{Y}^T]}{\sqrt{E\left[\boldsymbol{X}^2\right] E[\boldsymbol{Y}^2]}} \\ &= \frac{E[\boldsymbol{w}_x{}^T \boldsymbol{x}\boldsymbol{y}^T \boldsymbol{w}_y]}{\sqrt{E[\boldsymbol{w}_x{}^T \boldsymbol{x}\boldsymbol{x}^T w_x] E[\boldsymbol{w}_y{}^T \boldsymbol{y}\boldsymbol{y}^T \boldsymbol{w}_y]}}. \end{aligned} \tag{2}$$

Therefore, the maximum ρ with respect to $\boldsymbol{w}_x^T$ and $\boldsymbol{w}_y^T$ is the maximum canonical correlation. In this study, the source dataset (i.e., $\boldsymbol{x} \in \mathbb{R}^{N_c \times N_s}$) was SSVEPs, and the reference dataset (i.e., $\boldsymbol{y} \in \mathbb{R}^{2N_h \times N_s}$) was a combination of sinusoidal signals as follows:

$$\boldsymbol{y_n} = \begin{pmatrix} \sin(2\pi f_n t) \\ \cos(2\pi f_n t) \\ \vdots \\ \sin(2\pi N_h f_n t) \\ \cos(2\pi N_h f_n t) \end{pmatrix}, \; t = \frac{1}{f_s}, \frac{2}{f_s}, \ldots \frac{N_s}{f_s} \tag{3}$$

where f_n is the nth stimulus frequency, f_s is sampling rate, N_c is the number of channels, N_s is the number of data points, and N_h is the number of harmonics (was set to 3 in this study). In order to find the best electrode combination, the process of electrode selection was applied to recordings from each area. Eight electrodes were randomly selected for each area, and the SNRs were calculated using these electrodes after spatial filtering. The electrode selection was repeated 50 000 times for each area, and then the electrode combination that produces the highest SNR was noted and used for the following analysis.

2) Target Identification: This study also compared target identification accuracy and simulated ITRs using a 5-class SSVEP dataset measured from four different areas. The SSVEP signals were first down-sampled to 256 Hz. The performances were evaluated by the filter bank analysis proposed in [13] and the extended CCA analysis [4], [12] through a leave-one-out cross validation. The recorded EEG datasets were first decomposed into several sub-band components. The ith sub-band used the frequency range from the $i \times 8$ Hz to 70 Hz, which are designed according to our previous studies [13], [14]. The band-pass filters were realized with an infinite impulse response (IIR) filter. Zero-phase forward and reverse IIR filtering was implemented using the filtfilt() function in MATLAB. After applying the filter bank, an individual template $\widehat{\boldsymbol{x}}_n^{(i)}$ for nth visual stimulus and ith sub-band can be obtained by averaging multiple training trials in cross validation, and a test trial is denoted as $\boldsymbol{x}^{(i)}$. Correlation coefficients between projections of the test set and the template signals using CCA-based spatial filters can be used as features. Specifically, the following three weight coefficients were used as spatial filters: 1) $\boldsymbol{w}_{X\widehat{X}_n}^{(i)}$ between the test set $\boldsymbol{x}^{(i)}$ and the template signals $\widehat{\boldsymbol{x}}_n^{(i)}$; 2) $\boldsymbol{w}_{XY_n}^{(i)}$ between the test set $\boldsymbol{x}^{(i)}$ and the sine-cosine reference signals $\boldsymbol{y}_n$; 3) $\boldsymbol{w}_{\widehat{X}_nY_n}^{(i)}$ between the template signals $\widehat{\boldsymbol{x}}_n^{(i)}$ and the sine–cosine reference signals $\boldsymbol{y}_n$. In addition, the similarity between $\boldsymbol{w}_{X\widehat{X}_n}^{(i)}$ and $\boldsymbol{w}_{\widehat{X}_nX}^{(i)}$ was indirectly measured by calculating the correlation coefficient between the projections of template signals using the two spatial filters. A correlation vector $\boldsymbol{r}_n^{(i)}$ is defined as follows:

$$\boldsymbol{r}_n^{(i)} = \begin{bmatrix} r_{n,1}^{(i)} \\ r_{n,2}^{(i)} \\ r_{n,3}^{(i)} \\ r_{n,4}^{(i)} \\ r_{n,5}^{(i)} \end{bmatrix} = \begin{bmatrix} \rho\left(\left(\boldsymbol{w}_{XY_n}^{(i)}\right)^T \boldsymbol{x}^{(i)}, \left(\boldsymbol{w}_{Y_nX}^{(i)}\right)^T \boldsymbol{y}_n\right) \\ \rho\left(\left(\boldsymbol{w}_{X\widehat{X}_n}^{(i)}\right)^T \boldsymbol{x}^{(i)}, \left(\boldsymbol{w}_{X\widehat{X}_n}^{(i)}\right)^T \widehat{\boldsymbol{x}}_n^{(i)}\right) \\ \rho\left(\left(\boldsymbol{w}_{XY_n}^{(i)}\right)^T \boldsymbol{x}^{(i)}, \left(\boldsymbol{w}_{XY_n}^{(i)}\right)^T \widehat{\boldsymbol{x}}_n^{(i)}\right) \\ \rho\left(\left(\boldsymbol{w}_{\widehat{X}_nY_n}^{(i)}\right)^T \boldsymbol{x}^{(i)}, \left(\boldsymbol{w}_{\widehat{X}_nY_n}^{(i)}\right)^T \widehat{\boldsymbol{x}}_n^{(i)}\right) \\ \rho\left(\left(\boldsymbol{w}_{X\widehat{X}_n}^{(i)}\right)^T \widehat{\boldsymbol{x}}_n^{(i)}, \left(\boldsymbol{w}_{\widehat{X}_nX}^{(i)}\right)^T \widehat{\boldsymbol{x}}_n^{(i)}\right) \end{bmatrix} \quad (4)$$

where $\rho(a, b)$ indicates the correlation coefficient between a and b. The five correlation values were combined as follows:

$$\rho_n^{(i)} = \sum_{j=1}^{5} \text{sign}\left(r_{n,j}^{(i)}\right) \cdot {r_{n,j}^{(i)}}^2 \quad (5)$$

where a sigmoid function was used to retain discriminative information from negative coefficients between the test set and template signals. A weighted sum of squares of the combined correlation values corresponding to all sub-band components was calculated as the feature for target identification

$$\widetilde{\rho}_n = \sum_{i=1}^{I} \boldsymbol{W}(i) \cdot {\rho_n^{(i)}}^2 \quad (6)$$

where i is the index of the sub-band, I is the total number of sub-bands ($I = 5$ in this study), and $\boldsymbol{W}(i)$ was defined as $\boldsymbol{W}(i) = i^{-1.25} + 0.25$ according to [13]. The template signal that maximizes $\widetilde{\rho}_n$ was selected as the template signal corresponding to the target.

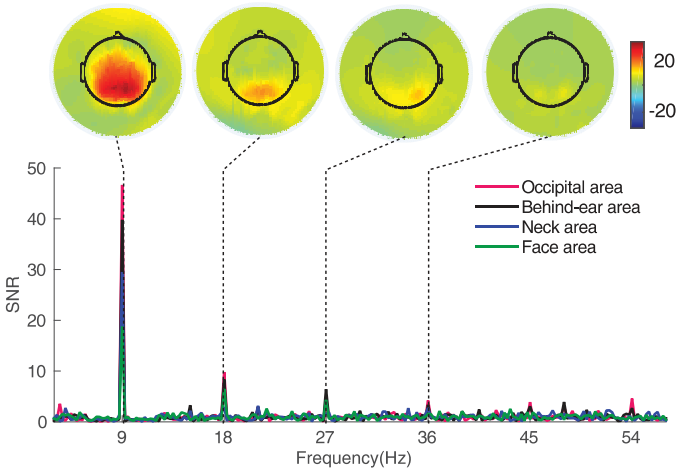

Fig. 3. SNR distribution of a sample subject gazing at a 9 Hz visual stimulus. The topographic maps at the top (left to right) panels are the 2-D SNR distribution at the fundamental frequency, second harmonics, third harmonics, and fourth harmonics, respectively.

III. Results

Fig. 3 shows that all of the four recording areas exhibit an SNR peak at the fundamental frequency (9 Hz) of the stimulus. The second, third, and fourth harmonics of SNR peaks are also appreciable. The top panels of Fig. 3 show 2-D scalp distributions of the SNRs of SSVEPs at the fundamental (9 Hz), the second harmonic, the third harmonic, and the fourth harmonic frequencies in response to 9 Hz stimulus (from left to right), respectively. Inferred from the two left-most scalp maps, the high SNRs (more red) appeared at the occipital area over the visual cortex, where, as expected, the source of SSVEPs is. The farther away from this area, the lower SNR (more green) an area could have, such as the face and neck areas. In the two right-most scalp maps, the SNR distribution is less explicit at the third and fourth harmonics, indicating lower SNR SSVEPs at the fourth harmonic over the neck, behind-the-ear, and face areas. Base on this finding, the online implementation used only the fundamental and the second harmonic for SSVEP detection, as described in detail in Section IV.

Fig. 4 shows the best SNR of each area after 50 000 iterations (i.e., randomly selects eight electrodes for each area) across 11 subjects. The resultant SNRs from low to high were from the face, neck, behind-the-ear, and occipital areas, which is consistent with our pilot study [22]. As the difference of the SNRs between the neck and the behind-the-ear areas was not statistically significant (Paired t-test, $p = 0.51$), only the signals from behind-the-ear area were used in the online SSVEP experiments described as follows.

Fig. 5 shows the average accuracy across all subjects for the five-target classification using the best combination of electrodes in each area across different data length from 1 to 4 s. In general, the accuracy of SSVEP detection increased as the data length increased. The occipital area achieved over 95% in classification accuracy even with a short data length.

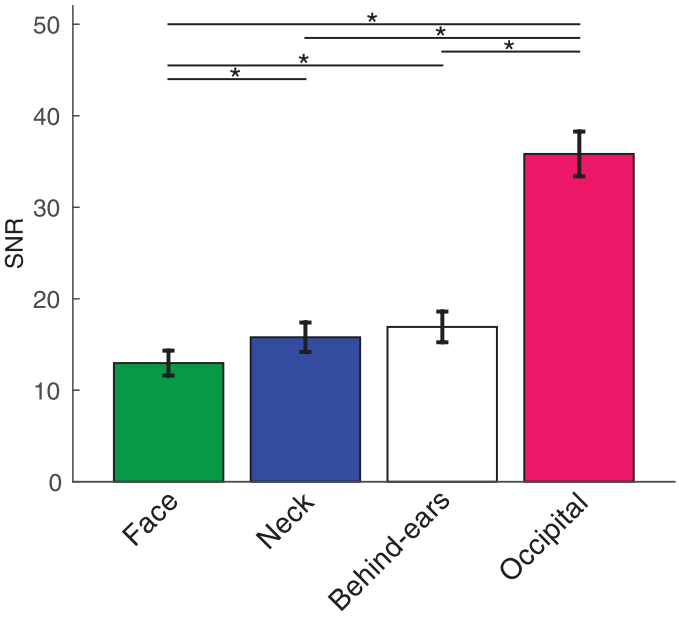

Fig. 4. Maximal SNR for each area across 11 subjects. Error bars indicate standard errors. The asterisks indicate significant difference between different areas ($*p < 0.05$).

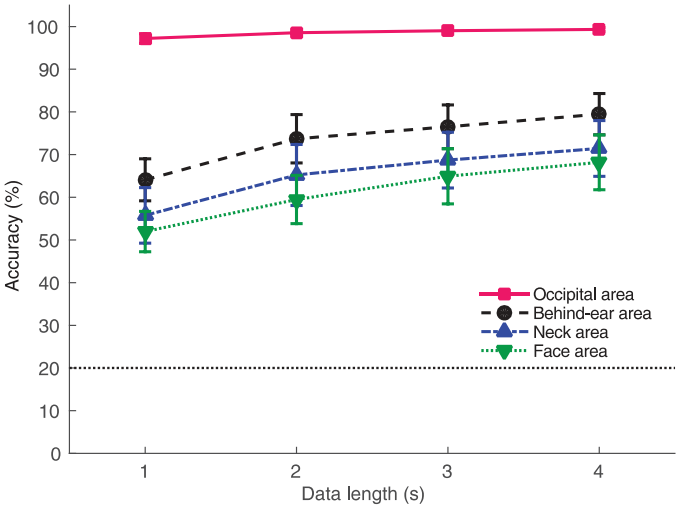

Fig. 5. Averaged classification accuracy across subjects using different electrode locations with different data lengths. Error bars indicate standard errors. The dotted line indicates chance-level accuracy in five-class classification.

The comparison of accuracy among behind-the-ear, neck, and face areas showed that the performance of the behind-the-ear area outperformed that of the neck area. One-way repeated measures analysis of variance (ANOVA) showed significant differences of the classification accuracy between these areas under all data length ($p < 0.05$). Although *post hoc* paired t-test did not show significant differences between behind-the-ear and neck areas, the accuracy of the behind-the-ear areas was higher than that of the neck area under all data length (behind the ear versus neck; 1 s: 64.10±4.93% versus 55.76± 6.51%, $p = 0.22$; 2 s: 73.71 ± 5.67% versus 65.23 ± 7.14%, $p = 0.16$; 3 s: 76.52±5.13% versus 68.71±6.52%, $p = 0.15$; 4 s: 79.47 ± 4.83% versus 71.44 ± 6.53%, $p = 0.12$).

In summary, results from high-density EEG recordings provided invaluable insights into the optimal channel selection:

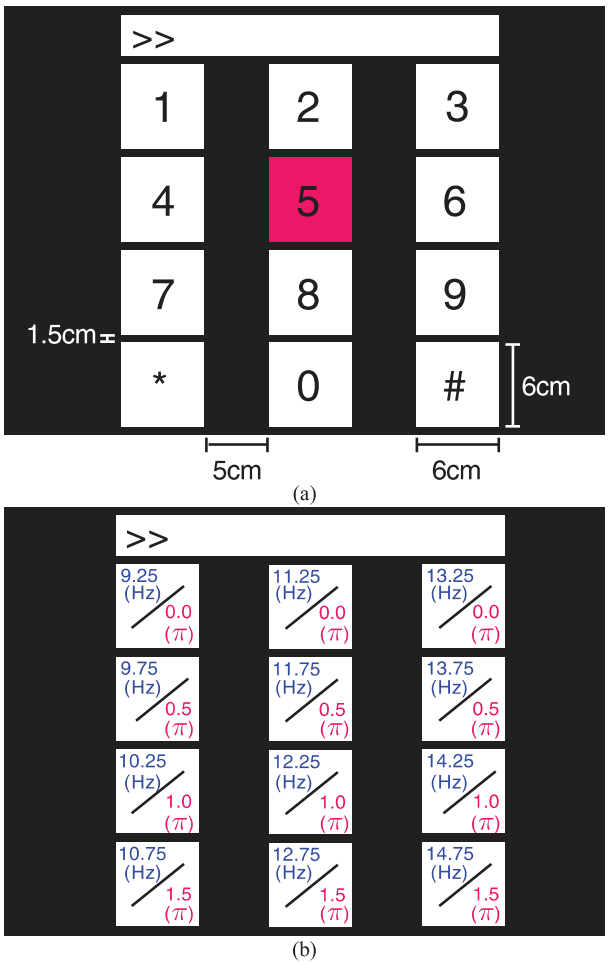

Fig. 6. Twelve-target stimulus matrix used in the online BCI experiment. (a) User interface in the experiment. (b) Frequency and phase values used for encoding each target in the stimulation matrix. Red square in (a) is the visual cue indicating a target symbol '5' in the experiment. Both figures were adapted from [27].

the electrodes near the occipital lobe (e.g., behind the ear and neck) were the best candidates to build an SSVEP-based BCI system based on non-hair-bearing montage. Considering that the muscle activities might contaminate the signals measured from the neck area, signals measured behind the ear areas seem to be the better choice of an online SSVEP-based BCI.

IV. Online Validation

A. Experimental Design

Twelve visual stimuli (each one consisted of a 6×6 cm square) were presented on a 27-in LCD monitor (ASUS VG278) with a refresh rate of 60 Hz and a resolution of 1280×800 pixels. As shown in Fig. 6, the stimuli were arranged in a 4×3 array similar to the keypad of a phone [16]. The horizontal and vertical intervals between two neighboring stimuli were 5 and 1.5 cm, respectively. In this study, the joint frequency and phase coding method, in which two adjacent targets are tagged with different frequencies and phases, was used to enhance the discriminability of each stimulus [9]. To be more specific, each stimulus was tagged with different frequencies (9.25 to 14.75 Hz with an interval of 0.5 Hz) and phases (0, 0.5π, π and 1.5π). The stimulation program

Fig. 7. Placements of four behind-the-ear electrodes while subjects performed the online SSVEP experiment.

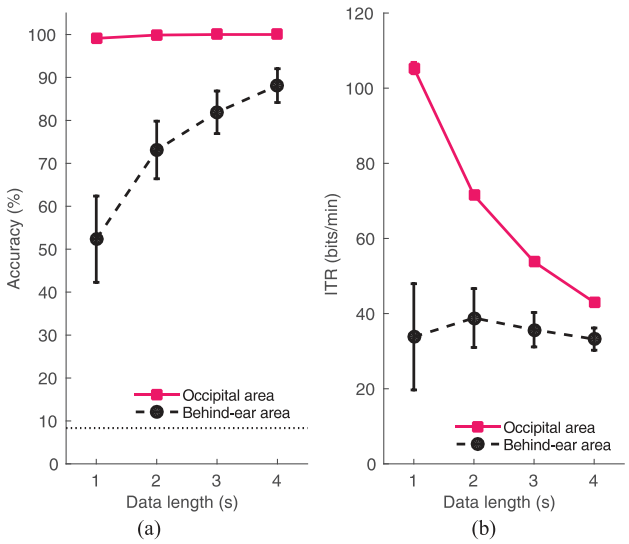

Fig. 8. (a) Classification accuracy and (b) ITRs of simulated online BCI experiments using the occipital and behind-the-ear electrodes with different data lengths. Error bars indicate standard errors. The dotted line in the bottom of (a) indicates chance-level accuracy in 12-class classification.

was developed on MATLAB (Mathworks, Inc.) using the Psychophysics Toolbox extensions [28].

Five subjects (five males and three of them did not participate in the offline experiments, mean age: 28.2 ± 1.92 years) with normal or corrected-to-normal vision participated in this online BCI study. They were asked to read and sign an informed consent form approved by the UCSD Human Research Protections before the experiment. They were seated in a comfortable chair and put their head on a chin rest that is 60 cm in front of the visual stimulator in a dim room. Eight Ag/AgCl electrodes were placed over the behind-the-ear areas (four on each side) to collect informative EEG signals, as shown in Fig. 7. Eight additional electrodes were placed over the occipital lobe as the gold standard for comparison. EEG signals were amplified and digitized at a sampling rate of 2048 Hz using BioSemi ActiveTwo EEG system (Biosemi, Inc.), and all electrodes were referenced to a forehead electrode. Event triggers that indicate the onsets of visual stimuli were sent and synchronized with EEG data in the amplifier.

B. Training Data Recording

This study performed a simulated online analysis for estimating the performance of BCIs [4], [29]. The experiment consisted of 15 bouts. Each bout consisted of 12 trials, in each trial subjects were asked to gaze at one of the targets for 4 s and then switched to the next target within 1 s. During this 1 s, the next target was rendered in red [i.e., #5 of Fig. 6(a)] as a cue. The cue appeared in a random order. To reduce eye-movement artifacts, subjects were asked to avoid blinks during the stimulation period.

C. Simulated Results

Data epochs comprising eight-channel SSVEPs over the occipital and the behind-the-ear areas, respectively, were extracted according to event triggers generated by the stimulus presentation program. All data epochs were down-sampled to 256 Hz. Considering a latency delay in the visual system, the data epochs were extracted in [0.135 s $0.135+d$ s], where the time zero indicated stimulus onset and d indicated data length used in the offline analysis. The 135-ms delay was selected towards the highest classification accuracy [14]. This study used a leave-one-out cross validation to estimate the target identification accuracy and the simulated ITR.

Fig. 8(a) and (b) shows the average accuracy and ITRs across all subjects with data length from 1 to 4 s, respectively. The target identification using the occipital area achieved nearly perfect accuracy even with short data length (1 s: 99.11 ± 0.62%, 2 s: 99.89 ± 0.11%, 3 s: 100.00 ± 0.00%, 4 s: 100.00±0.00%). The ITRs decline as the data length increased (1 s: 105.37 ± 1.51 bits/min, 2 s: 71.51 ± 0.19 bits/min, 3 s: 53.77±0.00 bits/min, 4 s: 43.02±0.00 bits/min). Although the accuracy using the behind-the-ear channels were not as high as that using the occipital channels (1 s: 52.33 ± 10.04%, 2 s: 73.11 ± 6.69%, 3 s: 81.89 ± 4.96%, 4 s: 88.11 ± 3.93%), the average accuracy using the behind-the-ear channels reached almost 90%. With 4 s-long data, the ITR using the behind-the-ear channels reached 33.22 ± 2.62 bits/min.

D. Online BCI Results

The truly online BCI experiment requires subjects to input a predetermined 12-symbol sequence without visual cues. Each subject performed three bouts with a short break in between. All 12 visual stimuli started to flicker simultaneously for 4 s on the monitor. During that time, subjects were asked to gaze at a target stimulus. They had to keep their gaze on the target until a red rectangle marked the position of the correct target stimulus identified by the online program. After that, subjects had 1 s to switch their gaze to the next target. Before the online experiment, every subject practiced for a few minutes to become familiar with the online task.

Table I lists the results of online BCI operation across the five subjects. The average accuracy was 84.08 ± 15.60%, leading to an average ITR of 30.21 ± 10.61 bits/min. Three subjects (Subjects 1, 4, and 5) achieved an accuracy over 90%, and subject 4 achieved 100% accuracy. Although the

TABLE I
ONLINE RESULTS

Subject	Total no. of trials (correct/ incorrect)	Completion time [s]	Accuracy [%]	ITR [bits/min]
S1	39 (36/3)	195	92.31	35.13
S2	47 (36/11)	235	76.60	23.88
S3	43 (36/7)	215	83.72	28.57
S4	36 (36/0)	180	100.00	43.02
S5	38 (36/2)	190	94.74	37.26
Mean±STD	-	-	84.08±15.60	30.21±10.61

ITR obtained in this study is not comparable to those reported in the previous results that used signals from the occipital electrodes, the results clearly suggested that signals measured from behind-the-ear electrodes could provide reliable SSVEPs for realizing an online BCI system.

V. DISCUSSION AND CONCLUSION

SSVEP-based BCIs have attracted increasing attention in recent years. However, most studies mainly focused on improving the performance (i.e., ITR and accuracy) in well-controlled laboratory environments. Transitioning laboratory demonstrations of SSVEP-based BCIs to real-world applications poses severe challenges on signal measuring and processing. For instance, long skin preparation and conduct-gel usage are some of the technical barriers of using SSVEP-based BCI systems in daily life. Despite the fact that dry electrodes, in-the-ear electrodes, and soft and curved auricle-based electrodes provide alternative approaches to reduce the preparation time and to avoid the usage of conduct gels, low ITRs make these advanced sensing technologies impracticable in real-life BCI applications.

This study conducted an offline and an online experiment to explore the feasibility of using electrodes placed over non-hair-bearing areas to build an SSVEP-based BCI system. The offline SSVEP experiments acquired signals from 256 electrodes populated across the whole head across 11 subjects. First, the SNR topographies showed that the elicited SSVEPs were indeed projected to the whole head, including the face, neck, and behind-the-ear areas. In general, the ranking of SNRs was occipital $>$ behind the ears $>$ neck $\approx$ face area, which was consistent with our previous finding [22]. Second, this study evaluated the five-class classification accuracy using leave-one-trial-out cross-validation. The resultant average accuracy using 4-s-length data was 79.47±4.83%, 71.44±6.53%, and 68.18±6.43% for the behind-the-ear, the neck, and the face area, respectively. Moreover, the study results showed that the SSVEPs at the fundamental and second harmonic frequencies were appreciable while the SSVEPs at higher harmonics were not visible in the signals measured from the non-hair-bearing areas. These empirical results suggested that using EEG signals from non-hair-bearing areas could be an alternative approach to realize an online SSVEP-based BCI. Third, five subjects successfully completed the truly online SSVEP tasks, in which each of them inputted 12 coded targets using EEG signals solely from eight electrodes placed over the behind-the-ear area. The averaged accuracy was 84.08 ± 15.60% and averaged ITR was 30.21±10.61 bits/min. Among the subjects, three achieved accuracy over 90% and one could achieve 100%.

Another important contribution of this work is to quantitatively compare the SSVEP target identification accuracy and ITRs obtained from non-hair areas with that obtained from the simultaneously recorded signals from occipital electrodes. The comparison provided a guideline for finding a balance between the advantages (accessibility) of and the disadvantages (reduced accuracy and ITRs) of non-hair EEG signals. Although the performance of the BCI with occipital SSVEPs is significantly better than that with non-hair SSVEPs, placing electrodes on non-hair area can be an alternative way for some users. Recording from hair-covered area is inconvenient. For example, for some patients who faced up and were lying on the bed, a non-hair BCI system might be a better choice since occipital area is difficult to access. However, the BCI with recordings on the occipital electrodes might be preferred for some users since the accuracy can be nearly 100%.

In summary, this study demonstrated the feasibility and practicality of using non-hair-bearing electrodes to build an online SSVEP-based BCI application. Possible future directions of this study could be reducing the number of non-hair-bearing electrodes, optimizing electrodes combinations, and increasing the number of targets in real-world BCI applications such as a BCI speller.

REFERENCES

[1] F. B. Vialatte, M. Maurice, J. Dauwels, and A. Cichocki, "Steady-state visually evoked potentials: Focus on essential paradigms and future perspectives," *Prog. Neurobiol.*, vol. 90, no. 4, pp. 418–438, 2010.
[2] J. R. Wolpaw, N. Birbaumer, D. J. McFarland, G. Pfurtscheller, and T. M. Vaughan, "Brain-computer interfaces for communication and control," *Clin. Neurophysiol.*, vol. 113, no. 6, pp. 767–791, 2002.
[3] X. Gao, D. Xu, M. Cheng, and S. Gao, "A BCI-based environmental controller for the motion-disabled," *IEEE Trans. Neural Syst. Rehabil. Eng.*, vol. 11, no. 2, Mar. 2003.
[4] M. Nakanishi, Y. Wang, Y.-T. Wang, Y. Mitsukura, and T.-P. Jung, "A high-speed brain speller using steady-state visual evoked potentials," *Int. J. Neural Syst.*, vol. 24, no. 6, p. 1450019, 2014.
[5] Y. Wang, Y.-T. Wang, and T.-P. Jung, "Visual stimulus design for high-rate SSVEP BCI," *Electron. Lett.*, vol. 46, no. 15, pp. 1057–1058, 2010.
[6] M. Nakanishi, Y. Wang, Y.-T. Wang, Y. Mitsukura, and T.-P. Jung, "Generating visual flickers for eliciting robust steady-state visual evoked potentials at flexible frequencies using monitor refresh rate," *PLoS One*, vol. 9, no. 6, p. e99235, 2014.
[7] X. Chen, Z. Chen, S. Gao, and X. Gao, "A high-ITR SSVEP based BCI speller," *Brain-Comp. Interfaces*, vol. 1, no. 3–4, pp. 181–191, 2014.
[8] Y.-T. Wang, Y. Wang, C.-K. Cheng, and T.-P. Jung, "Developing stimulus presentation on mobile devices for a truly portable SSVEP-based BCI," in *Proc. Ann. Int. Conf. IEEE Eng. Med. Biol. Soc.*, 2013, pp. 5271–5274.
[9] X. Chen, Y. Wang, M. Nakanishi, T.-P. Jung, and X. Gao, "Hybrid frequency and phase coding for a high-speed SSVEP-based BCI speller," in *Proc. Ann Int. Conf. IEEE Eng. Med. Biol. Soc.*, 2014, pp. 3993–3996.
[10] Z. Lin, C. Zhang, W. Wu, and X. Gao, "Frequency recognition based on canonical correlation analysis for SSVEP-based BCIs," *IEEE Trans. Biomed. Eng.*, vol. 54, no. 6, pp. 1172–1176, Jun. 2007.
[11] G. Bin, X. Gao, Z. Yan, B. Hong, and S. Gao, "An online multi-channel SSVEP-based brain-computer interface using a canonical correlation analysis method," *J. Neural Eng.*, vol. 6, no. 4, p. 046002, 2009.
[12] Y. Wang, M. Nakanishi, Y.-T. Wang, and T.-P. Jung, "Enhancing detection of steady-state visual evoked potentials using individual training data," in *Proc. Ann. Int. Conf. IEEE Eng. Med. Biol. Soc.*, 2014, pp. 3037–3040.
[13] X. Chen, Y. Wang, S. Gao, T.-P. Jung, and X. Gao, "Filter bank canonical correlation analysis for implementing a high-speed SSVEP-based brain-computer interface," *J. Neural Eng.*, vol. 12, no. 4, p. 046008, 2015.

[14] X. Chen, Y. Wang, M. Nakanishi, X. Gao, T.-P. Jung, and S. Gao, "High-speed spelling with a noninvasive brain-computer interface," *Proc. Nat. Acad. Sci. USA*, vol. 112, no. 44, pp. E6058–E6067, 2015.
[15] Y. Wang, X. Gao, B. Hong, C. Jia, and S. Gao, "Brain-computer interfaces based on visual evoked potentials: Feasibility of practical system design," *IEEE Eng. Med. Biol. Mag.*, vol. 27, no. 5, pp. 64–71, 2008.
[16] Y.-T. Wang, Y. Wang, and T.-P. Jung, "A cell-phone based brain computer interface for communication in daily life," *J. Neural Eng.*, vol. 8, no. 2, p. 025018, 2011.
[17] Y. M. Chi, Y.-T. Wang, Y. Wang, C. Maier, T.-P. Jung, and G. Gauwenberghs, "Dry and noncontact EEG sensors for mobile brain-computer interfaces," *IEEE Trans. Neural Syst. Rehabil. Eng.*, vol. 20, no. 2, pp. 228–235, Mar. 2012.
[18] F. N.-A. Luis and G.-G. Jaime, "Brain computer interfaces, A review," *Sensors*, vol. 12, no. 2, pp. 1211–1279, 2012.
[19] K. McDowell, C.-T. Lin, K. S. Oie, T.-P. Jung, S. Gordon, K. W. Whitaker, S.-Y. Li, S.-W. Lu, and W. D. Hairston, "Real-world neuroimaging technologies," *IEEE Access*, vol. 1, pp. 131–149, 2013.
[20] Y. M. Chi, T.-P. Jung, and G. Cauwenberghs, "Dry-contact and noncontact biopotential electrodes: Methodological review," *IEEE Rev. Biomed. Eng.*, vol. 3, pp. 106–119, 2010.
[21] D. Regan, *Human Brain Electrophysiology: Evoked Potentials and Evoked Magnetic Fields in Science and Medicine*. New York, NY, USA: Elsevier, 1989, p. 672.
[22] Y.-T. Wang, Y. Wang, and T.-P. Jung, "Measuring steady-state visual evoked potentials from non-hair-bearing areas," in *Proc. Ann. Int. Conf. IEEE Eng. Med. Biol. Soc.*, 2014, pp. 1806–1809.
[23] Y.-T. Wang *et al.*, "Developing an online steady-state visual evoked potential-based brain-computer interface system using EarEEG," in *Proc. Ann. Int. Conf. IEEE Eng. Med. Biol. Soc.*, pp. 2271–2274, 2015.
[24] J. J. S. Norton *et al.*, "Soft, curved electrode systems capable of integration on the auricle as a persistent brain-computer interface," *Proc. Nat. Acad. Sci. USA*, vol. 112, no. 13, 2015.
[25] Y. Wang, R. Wang, X. Gao, B. Hong, and S. Gao, "A practical VEP-based brain-computer interface," *IEEE Trans. Neural Syst. Rehabil. Eng.*, vol. 14, no. 2, pp. 234–239, Mar. 2006.
[26] A. Delorme and S. Makeig, "EEGLAB: An open source toolbox for analysis of single-trial EEG dynamics including independent component analysis," *J. Neurosci. Methods*, vol. 134, no. 1, pp. 9–21, 2004.
[27] M. Nakanishi, Y. Wang, Y.-T. Wang, and T.-P. Jung, "A comparison study of canonical correlation analysis based methods for detecting steady-state visual evoked potentials," *PLoS One*, vol. 10, no. 10, p. e0140703, 2015.
[28] D. H. Brainard, "The psychophysics toolbox," *Spat. Vis.*, vol. 10, no. 4, pp. 433–436, 1997.
[29] C. Jia, X. Gao, B. Hong, and S. Gao, "Frequency and phase mixed coding in SSVEP-based brain-computer interface," *IEEE Trans. Biomed. Eng.*, vol. 58, no. 1, pp. 200–206, Jan. 2011.

Yu-Te Wang (S'15-M'16) received the M.S. degree from National Chiao Tung University, Hsinchu, Taiwan, in 2009, and the Ph.D. degree in computer science and engineering at the University of California San Diego, La Jolla, in 2015.

Currently, he is a Staff Research Associate III at the Swartz Center for Computational Neuroscience, University of California San Diego. His research interests include brain-computer interface and biomedical signal processing.

Masaki Nakanishi (S'10-M'14) received the B.E. and M.E degrees from Tokyo University of Agriculture and Technology, Tokyo, Japan, in 2009 and 2010, respectively, and the Ph.D. degree in engineering from Keio University, Kanagawa, Japan, in 2014.

He was a Research Fellow of Japan Society for the Promotion of Science, Japan, in 2013 through 2015. He is currently a Postdoctoral Researcher at the Hamilton Glaucoma Center, Department of Ophthalmology and the Swartz Center for Computational Neuroscience, University of California San Diego. His research interests include brain-computer interface and biomedical signal processing.

Yijun Wang (M'11) received the B.E. and Ph.D. degrees in biomedical engineering from Tsinghua University, Beijing, China, in 2001 and 2007, respectively.

From 2008 to 2015, he was first a Postdoctoral Fellow and then an Assistant Project Scientist at the Swartz Center for Computational Neuroscience, University of California San Diego, USA. He is currently a Research Fellow at Institute of Semiconductors, Chinese Academy of Sciences, Beijing, China. His research interests include brain-computer interface, biomedical signal processing, and machine learning.

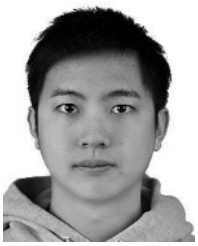

Chun-Shu Wei (S'15) received the B.S. degree in electrical engineering and computer science and the M.S. degree in electrical engineering from National Chiao Tung, Hsinchu, Taiwan, in 2009 and 2011 respectively. He is currently working toward the Ph.D. degree in bioengineering at the University of California San Diego.

His research interests include brain-computer interface, biomedical signal processing, and machine learning.

Chung-Kuan Cheng (S'82-M'84-SM'95-F'00) received the B.S. and M.S. degrees in electrical engineering from National Taiwan University, and the Ph.D. degree in electrical engineering and computer sciences from University of California, Berkeley, CA, USA, in 1984.

From 1984 to 1986, he was a Senior CAD Engineer at Advanced Micro Devices Inc. In 1986, he joined the University of California, San Diego, where he is a Distinguished Professor in the Computer Science and Engineering Department, an Adjunct Professor in the Electrical and Computer Engineering Department. He served as a Principal Engineer at Mentor Graphics in 1999. His research interests include medical modeling and analysis, network optimization and design automation on microelectronic circuits.

Dr. Cheng is a recipient of the best paper awards, IEEE Transactions on Computer-Aided Design in 1997, and in 2002, the NCR excellence in teaching award, School of Engineering, UCSD in 1991, IBM Faculty Awards in 2004, 2006, and 2007, the Distinguished Faculty Certificate of Achievement, UJIMA Network, UCSD in 2013. He has been appointed as an Honorary Guest Professor of Tsinghua University 2002 through 2008, and a Visiting Professor of National Taiwan University, in 2011 and 2015. He was an Associate Editor of IEEE Transactions on Computer–Aided Design from 1994 to 2003.

Tzyy-Ping Jung (S'91-M'92-SM'06-F'15) received the B.S. degree in electronics engineering from National Chiao Tung University, Hsinchu, Taiwan, in 1984, and the M.S. and Ph.D. degrees in electrical engineering from The Ohio State University, Columbus, OH, USA, in 1989 and 1993, respectively.

He is currently a Research Scientist and the Co-Director of the Center for Advanced Neurological Engineering, Institute of Engineering in Medicine, University of California-San Diego (UCSD), La Jolla, CA, USA. He is also an Associate Director of the Swartz Center for Computational Neuroscience, Institute for Neural Computation, and an Adjunct Professor of Bioengineering at UCSD. In addition, he is an Adjunct Professor of Computer Science, National Chiao Tung University, Hsinchu, Taiwan. His research interests are in the areas of biomedical signal processing, cognitive neuroscience, machine learning, time frequency analysis of human EEG, functional neuroimaging, and brain–computer interfaces and interactions.